CHIN. PHYS. LETT. Vol. 38, No. 3 (2021) 038102

Au Films Composed of Nanoparticles Fabricated on Liquid Surfaces for SERS

Xunheng Ye(叶迅亨), Jiawei Shen(沈佳伟), Xiangming Tao(陶向明), Gaoxiang Ye(叶高翔), and Bo Yang(杨波)*

Department of Physics, Zhejiang University, Hangzhou 310027, China

(Received 28 October 2020; accepted 23 December 2020; published online 2 March 2021)

A series of Au films with different nominal deposition thickness d were fabricated on ionic liquid surfaces by thermal evaporation at room temperature, taken as surface-enhanced Raman scattering (SERS) substrates. Au atoms deposited on the liquid surfaces can diffuse and aggregate randomly and eventually form films with ramified structure, which consist of nanoparticles (NPs). There are amounts of ultrasmall (∼1 nm or smaller) nanogaps among the Au NPs, which can dramatically enhance Raman signal. Raman spectra of R6G were investigated with the assistance of the Au films. The results indicate that the Au films with higher thickness possess better SERS performance when $5.0 \leq d \leq 30.0$ nm. A random distribution model of Au NPs was used in the finite-difference time-domain method and the simulation results are in good agreement with the experimental findings.

DOI: 10.1088/0256-307X/38/3/038102

The Raman scattering signals of molecules near the surface of noble metal such as silver (Ag) or gold (Au) can be greatly enhanced.[1] This interesting phenomenon is called surface-enhanced Raman scattering (SERS). Influenced by the various structure and characteristic SERS substrates, SERS can detect the signals of low concentration samples, which cannot be measured by the normal Raman spectra. It even can be used to monitor the signals of single molecules.[2–4] Thanks to its great advantage in signal amplification, SERS possesses wide applications in areas such as chemics,[5] biology,[6,7] and nanomedicine.[8,9] Although there are a lot of mysteries about the mechanism of SERS, it is generally realized that there are two main effects that contribute to the great ability of signal increasing: electromagnetic (EM) and chemical effects.[2] The former enhancement are caused by the localized surface plasma resonance (LSPR) in nanostructured metals[10,11] and the later enhancement arises from the transfer of electrons between adsorbed molecules and substrates.[12]

In 1998, Ye *et al.* presented the results on the formation of Ag films on silicone oil surfaces by thermal evaporation method.[13] Since then, many metallic films with different morphologies and nanostructures have been fabricated on various kinds of liquid substrates successfully.[14–17] Generally, liquid surfaces can be considered as isotropic and quasi-free sustained substrates, and possess the characteristics of quasi-atomically smooth surfaces.[18] Therefore, the metallic atoms deposited on the liquid surfaces can diffuse randomly with large diffusion coefficients at room temperature. Owing to the specific characteristics of the liquid surfaces, nanoparticles (NPs) can be easily formed on the liquid surfaces and then aggregate to form films containing ramified aggregates.[13,19,20] Both the microstructure and growth mechanism of metallic films are quite different from those on solid substrates.

In this Letter, Au films deposited on ionic liquid surfaces are utilized as SERS substrates. The influence factor of SERS performance of the Au films and the feasibility of these substrates for practical applications are studied. Rhodamine 6G (R6G) with different concentrations are used as probe molecules to evaluate the SERS performance of the prepared Au films. Our experimental results show that the Raman intensities are dramatically enhanced with the assistance of the substrates. The finite-difference time-domain (FDTD) method[21–23] is utilized to simulate the electric field distribution among the Au NPs and to analyze the influence of number density of the Au NPs on SERS performance. The simulation results indicate that, under the condition of $5.0 \leq d \leq 30.0$ nm, the electric field intensity may be strongly enhanced as the number density of metallic NPs increases, which is consistent with the experimental observations.

Experimental Methods. The Au films were fabricated by thermal evaporation in a vacuum of 3.0×10^{-6} mbar at room temperature ($T = 25 \pm 2$ ℃). An ionic liquid (1-butyl-3-methylimidazolium tetrafluoroborate, purity, 99%+, adamas) was used as the liquid substrate, which was uniformly painted onto a 10×10 mm^2 frosted glass surface with resulting liquid substrate thickness of around 0.5 mm. Then the liquid substrate was placed in the vacuum chamber near a quartz-crystal balance (ULVAC CRTM), which could monitor the deposition rate f and the nominal deposition thickness d. Au wires (purity, 99.99%+) were wrapped around a portion of the tungsten filament 130 mm above the liquid substrate. In our experiments, the deposition rate f was fixed at 0.02 nm/s and the nominal deposition thickness d varied from 5.0 to 30.0 nm.

After deposition, the prepared Au films were kept

Supported by the National Natural Science Foundation of China (Grant No. 11374082).
*Corresponding author. Email: boyang@zju.edu.cn
© 2021 Chinese Physical Society and IOP Publishing Ltd

in the vacuum chamber for 15 min and then removed out from the chamber. Subsequently, the Au films were transferred from the ionic liquid surfaces to polished silicon wafers through the following method: a silicon wafer cleaned by ultrasonic was used to cover on the prepared Au film surface for 10 min, so that the Au film may adhere the silicon wafer surface tightly. Then the wafer stuck with the Au was washed carefully by acetone, ethanol and deionized water repeatedly until the ionic liquid was cleaned.[18]

The microstructures of the Au films were measured by a scanning electron microscopy (SEM, Zeiss Supra 55). Then, the Au films were utilized as SERS substrates and the R6G was used as the probe molecule. The samples were coated with the R6G through immersion in the R6G aqueous solution with different concentration c for 20 min, followed by rinsing with ethanol and drying at room temperature. All the Raman spectra were measured under 532 nm continuous-wave laser excitation using an Andor SR-500i-B1 spectrograph. The Raman spectra were collected using 50× objective lens. The laser power was set to 2.1 mW. The diameter of laser spot was about 2 μm and the signal integration time for each measurement was 10 s.

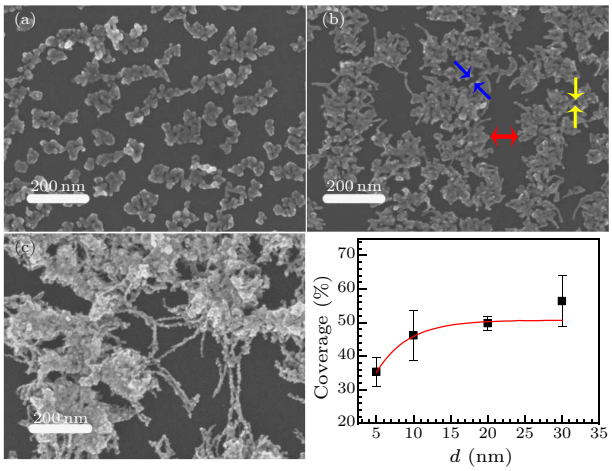

Fig. 1. SEM images of the Au films deposited on ionic liquid surfaces with nominal thickness of (a) $d = 5.0$ nm, (b) $d = 10.0$ nm and (c) $d = 30.0$ nm, respectively; (d) the evolution of the coverage of the Au films with d and the red curve is the guide to the eyes.

Results and Discussion. Figures 1(a)–1(c) show the morphologies and microstructures of the Au films with nominal thickness d ranging from 5.0 to 30.0 nm. It is revealed that the Au films are composed of ramified Au aggregates, which formed and randomly distributed on the ionic surfaces and were well transferred to the polished silicon surfaces. The size and branch width of the ramified aggregates increase with d. The SEM images in Figs. 1(a)–1(c) also show that the ramified aggregates are composed of Au NPs with the size about 10–20 nm and the average distance between each adjacent two Au NPs decreases with the thickness d. Figure 1(d) shows that the surface coverage of the Au aggregates increases with d and tends to saturation gradually.

An interesting phenomenon is that there are numerous large gaps [red arrow in Fig. 1(b)] with characteristic size about 10^2 nm between two aggregates and small nanogaps [blue arrow in Fig. 1(b)] and nanopores [yellow arrow in Fig. 1(b)] with characteristic size about 10 nm inside the aggregates. Unexpectedly, there are some beard structures at the edge of the Au aggregates in Figs. 1(b) and 1(c), which grow gradually as d increases. This typical structure has never been observed before.[14,19] We propose that both the ramified and the beard structured aggregates may be formed by different self-assembly modes of Au NPs on the liquid surfaces.

According to the experimental results above, we may propose that the formation mechanism of the microstructure of the Au films shown in Fig. 1 may basically described by the two-stage growth model.[13] The deposition Au atoms firstly nucleate and grow into NPs, then the NPs diffuse randomly on the liquid surface to form ramified aggregates and the surface coverage increases with the thickness d. As d further increases, the NPs in the ramified aggregates tend to be more and more closely integrated with each other, resulting in the saturation coverage value of the Au aggregates shown in Fig. 1(d).

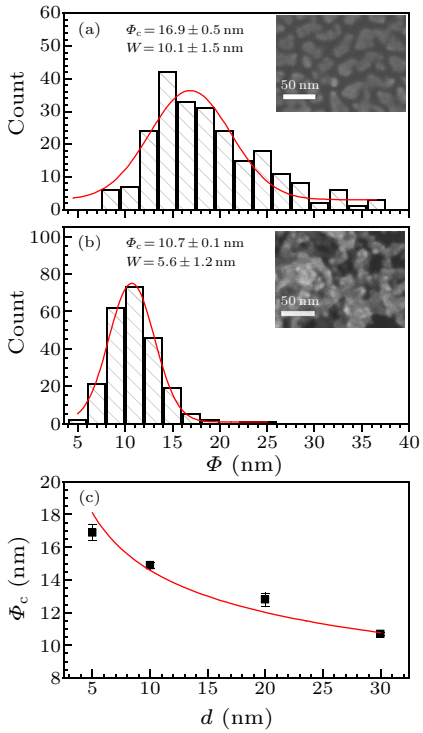

Fig. 2. The statistic distribution histograms of the Au NPs sizes, (a) $d = 5.0$ nm and (b) $d = 30.0$ nm, respectively. (c) The evolution of the most probable size of the distribution Φ_c with d.

For further investigating the microstructure of the samples, statistical measurements for the diameters of the NPs Φ are performed. The distributions of Φ is found to be resemble a rough Gaussian distribution as shown in Fig. 2, in which, Φ_c, the peak value

of the distribution, decreases from 16.9 ± 0.5 nm to 10.7 ± 0.1 nm and W, the full width at half maximum, decreases from 10.1 ± 1.5 nm to 5.6 ± 1.2 nm as d increases from 5.0 nm to 30.0 nm. The fitting curve in Fig. 2(c) shows that Φ_c decreases with d and flattens out gradually, which may associate with the material aggregation and structural collapse in the three-dimension growth process.[24]

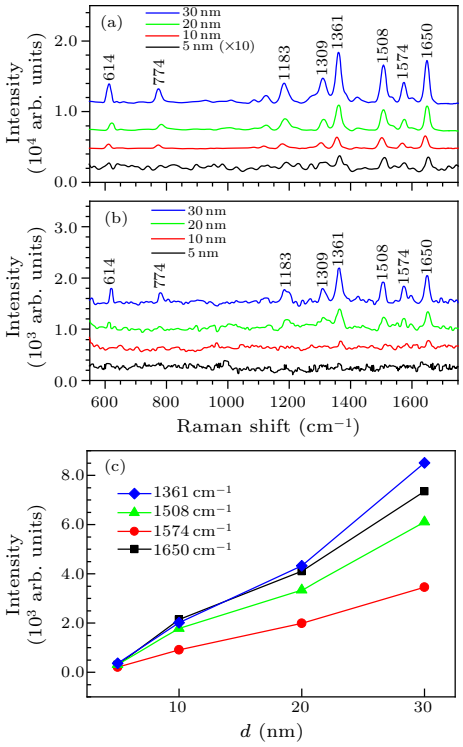

Fig. 3. Raman spectrum of R6G with the assistance of the Au films. The samples were immersed in different concentrations of R6G solution: (a) $c = 1 \times 10^{-4}$ M and (b) $c = 1 \times 10^{-7}$ M. (c) Intensities of Raman characteristic peak of 1×10^{-4} M versus d.

In order to evaluate the SERS performance of the Au films, the Raman spectrum of R6G with assistance of the Au films is shown in Fig. 3. This experimental result has been verified by repeated experiments. The concentrations of R6G in Figs. 3(a) and 3(b) are 10^{-4} M and 10^{-7} M, respectively. It can be seen that the characteristic peaks of R6G are detected on all prepared Au substrates with difference thicknesses. The dependence between the Raman intensities of 10^{-4} M and d can be seen in Fig. 3(c). Obviously, all the intensities of the characteristic peaks at 1361 cm^{-1}, 1508 cm^{-1}, 1574 cm^{-1} and 1650 cm^{-1} increase with d. It is noted that the Au films with $d = 30$ nm possesses the best performance in our experiments, as shown in Fig. 3(c). An important phenomenon is that the characteristic peaks of R6G in the samples with $d \geq 10$ nm can still be identified at the concentration as low as 10^{-7} M, which indicates the high efficiency of the Au substrates for the SERS detection.

In general, the size of the Au NPs may influence the SERS performance of Au films.[25,26] However, both the number density of the Au NPs inside the ramified aggregates and the ultrasmall (∼1 nm or smaller) nanogaps among the Au NPs play a more important role in SERS performance.[3,27] In order to theoretically elucidate the effect of the Au NPs number density on SERS enhancement, a random distribution of the Au NPs model was established and its electric field distribution was calculated using the FDTD method, as shown in Fig. 4. The Au NPs with diameter of 10 nm are randomly distributed in a square of 100×100 nm^2. The numbers of the Au NPs, namely N, in Figs. 4(a) and 4(c) are $N = 10$ and $N = 40$, respectively. Figures 4(b) and 4(d) give the relative enhanced electric field E/E_0 distribution corresponding to the model shown in Figs. 4(a) and 4(c), respectively, where E_0 and E are the amplitudes of the incident and enhanced electric fields, respectively. Generally, E/E_0 can roughly reflect the Raman enhancement effect.[22]

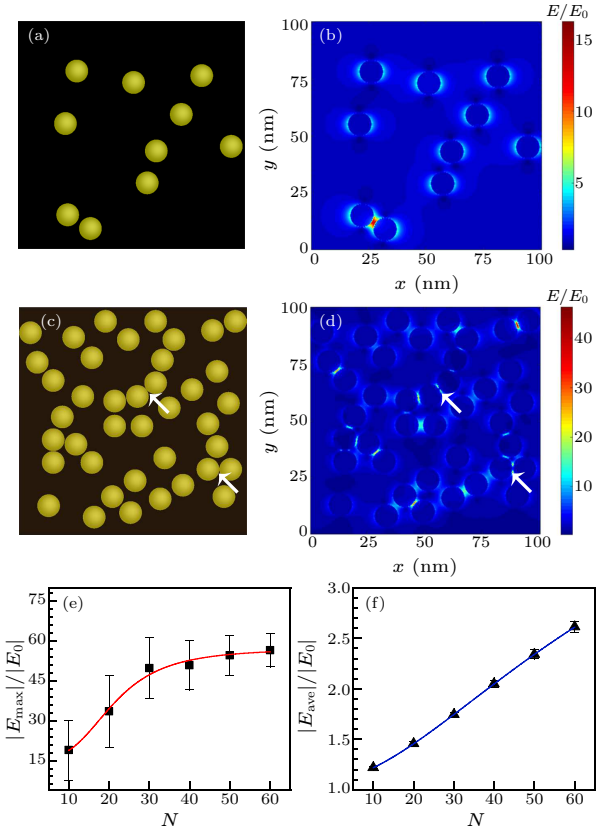

Fig. 4. Simulation of the FDTD model for the electric field enhancement of the randomly distributed Au NPs. The numbers of the NPs are (a) $N = 10$ and (c) $N = 40$; (b) and (d) represent the electric field distributions corresponding to (a) and (c), respectively. The color bar E/E_0 indicates the electric filed enhancement; (e) and (f) represent the maximum electric field and average electric field versus N.

From Figs. 4(b) and 4(d), it can be seen that very strong electric fields appear in the narrow gap among the Au NPs when the gap size approaches about 1 nm, which is the so-called "hot spot".[28] Both the number of the hot spot and the electric field intensities in the hot spot increase with N. Previous studies[21] showed that the molecules located in the hot spot may get a

tremendous signal enhancement, because of the great electric enhancement effect. It is interesting to note that, as N goes up and the gap size is close to about 1 nm, the electric enhancement effect increases obviously. On the other hand, the electric field decreases when the gap width approaches zero, as shown by the arrows in Figs. 4(c) and 4(d). This phenomenon indicates that there should exist an optimal gap size l_0 for the best SERS performance. In addition, it can be seen in Fig. 4(b) that the edges of the isolated Au NPs may also make contribution to the enhancement of the electric field. However, this enhancement effect is much smaller than that of the hot spots.

The dependence between N and the ratio of the maximum electric field $E_{\max}$ to E_0 is shown in Fig. 4(e), in which each data point is obtained by averaging the results of 10 simulations with different random distributions (for the same N value) of the Au NPs. It can be seen that $|E_{\max}|/|E_0|$ tends to increase with N first, and then saturates gradually. Generally, proper separation between two adjacent NPs can greatly influence the enhancement effect.[3,21] If N increases gradually, the NPs approach each other. Then some of the distances between two adjacent NPs start to reach l_0 and then to obtain the maximum electric field enhancement effect. After that, $|E_{\max}|/|E_0|$ approaches saturation gradually. Therefore, the result shown in Fig. 4(e) is consistent with the previous findings.[3,21]

In fact, the average enhancement may more veritably and more fully reflect the overall enhancement of substrates. The dependence of the ratio of the average electric field E_{ave} to E_0 with N is shown in Fig. 4(f), where E_{ave} is obtained by averaging all data points in each of the electric field distribution maps, as shown in Figs. 4(b) and 4(d) for instance. It is noticed that E_{ave} increases with N for $N \leq 60$ and there is no trend towards saturation, as shown in Fig. 4(f), which is similar to the result published previously.[27] In simulation, we find that, after $E_{\max}$ approaches saturation, the number of the hot spots increases with N, which results in the phenomenon in Fig. 4(f) that E_{ave} linearly increases with N approximately. Another important phenomenon shown in Figs. 4(e) and 4(f) is that E_{ave} is much smaller than $E_{\max}$. This result indicates that the contribution to electric field enhancement from the area outside of the hot spots is small, and only the molecules in the area of the hot spots may produce strong signal enhancement. This conclusion is in good agreement with the previous findings.[21,29]

For comparison, an aggregation of Au NPs with a two-dimensional hexagonal close-packed structure was simulated by FDTD to analyze the electric field enhancement effect. The number of the Au NPs is $N = 105$. The simulation shows that $|E_{\max}|/|E_0| = 42.1$ and $|E_{\text{ave}}|/|E_0| = 2.35$, both are smaller than the corresponding values of 56.5 ± 6.2 and 2.61 ± 0.06 in the randomly distribution model with $N = 60$, respectively. As mentioned above, the electric field between the two adjacent NPs decreases when the gap width approaches zero in the simulation. Therefore, it is reasonable to see that $|E_{\max}|/|E_0|$ decreases when N approaches the maximum value in the hexagonal close-packed model, i.e., $N = 105$, which results in the decrease of $|E_{\text{ave}}|/|E_0|$. The simulation results above are in agreement with the experimental observations shown in Fig. 3 and indicate that, as N further increases, the performance of the Au NPs in electric field enhancement may even degrade if N goes beyond the critical value N_{c}.

The lager Raman enhancement of the Au films should originate from the following aspects: the ramified structure, and the Au NPs with ultrasmall (∼1 nm or smaller) nanogaps morphology. The ramified Au films can be regarded as the Au films consisting of many separated irregular Au islands. It was reported that the island structure possesses better SERS performance than continuous structure and smaller structural dimension can get larger EM enhancement.[30] Moreover, the ramified Au aggregates possess amounts of 10^1 order small gaps and nanopores inside the aggregates, which may also enhance the Raman signal by generating considerable EM fields.[31] However, different from the previous studies,[30] the Au films with larger branch width of the ramified aggregates exhibit better SERS performance in our experiments. Therefore, combining with the simulation results, we propose that the amounts of ultrasmall nanogaps among the NPs in the Au aggregates may be the main reason for the signal enhancement.

The ultrasmall nanogaps among the NPs can serve as the hot spots to greatly increase the signal in Raman detection.[3] It should be mentioned that the overall signal enhancement depends heavily on N, i.e., the total number of the Au NPs. Experimentally, N and the number density of the Au NPs increase with the increase of d, which results in the decrease of the average distance among the Au NPs. According to the simulation results, when N as well as the number density increases, more and stronger hot spots may form, which is beneficial to bring about higher enhancement effect. Therefore, the SERS performances of the Au films shown in Fig. 3 increase with d, which are in good agreement with the simulation results, and the optimal d of the Au films for the best SERS performance is $d \geq 30$ nm.

In summary, we have fabricated Au films on the ionic liquid surfaces by the thermal evaporation method as SERS substrates. Thanks to the specific characteristics of the ionic liquid surfaces, the ramified Au aggregates consisting of various Au NPs form on the liquid surfaces. There are amounts of ultrasmall nanogaps (around 1 nm or less) among the NPs in the aggregates. Both the ramified structure and the ultrasmall nanogaps of the films contribute to the great SERS performance of the Au films. We propose that the ultrasmall nanogaps may play a more important role in the signal enhancement in our experiments.

A random-distribution Au NPs model has been established in the FDTD simulation, and the results

are in good agreement with the experimental findings. The ultrasmall nanogaps can serve as the hot spots, which may greatly enhance the signal in Raman detection. As d increases, more and stronger hot spot may form in the Au films. Our experimental measurement indicates that the Au films with $d = 30$ nm exhibit the best SERS performance, which is in agreement with the simulation result. The FDTD simulation also indicates that the contribution from the area outside of the hot spots to the signal enhancement is less relatively. Therefore, we propose that designing and manufacturing the SERS substrates with more and stronger hot spots are key steps to improve the SERS performance of the films.

There are several advantages of the method given above. Firstly, various metallic films containing various NPs may be fabricated on different liquid surfaces and the size of the NPs may be controlled effectively. Secondly, it is quite easy to transfer the films from the liquid surfaces to other solid substrates. Finally, compared to some chemical preparation methods, fabricating metal films on liquid surfaces by the thermal evaporation is less consumable and more environmental friendly. Therefore, it is quite expected that, combining with the relatively excellent SERS performance, the noble metallic films deposited on liquid surfaces may become promising candidates for detection of small molecule analytes in the near future.

The authors sincerely thank Quanlin Ye, Huizhen Wu, Lu Li, Zhilong Bao and Fengyun Xu for useful discussions and technical assistance.

References

[1] Albrecht M G and Creighton J A 1977 *J. Am. Chem. Soc.* **99** 5215
[2] Kneipp K, Wang Y, Kneipp H, Perelman L T, Itzkan I, Dasari R and Feld M S 1997 *Phys. Rev. Lett.* **78** 1667
[3] Nam J M, Oh J W, Lee H and Suh Y D 2016 *Acc. Chem. Res.* **49** 2746
[4] Nie S M and Emery S R 1997 *Science* **275** 1102
[5] Kleinman S L, Frontiera R R, Henry A I, Dieringer J A and Van Duyne R P 2013 *Phys. Chem. Chem. Phys.* **15** 21
[6] Harroun S G, Abraham T J, Prudhoe C, Zhang Y, Scammells P J, Brosseau C L, Pye C C and Singer R D 2013 *Phys. Chem. Chem. Phys.* **15** 19205
[7] Karaballi R A, Nel A, Krishnan S, Blackburn J and Brosseau C L 2015 *Phys. Chem. Chem. Phys.* **17** 21356
[8] Li J H, Zhang S N, Zhai Y J, Ma J G, Fang W H and Zhang Y 2019 *Acta Phys. Sin.* **68** 134203 (in Chinese)
[9] Shin D M, Nie S, Qian X, Young A N, Wang M D, Ansari D O, Chen G Z, Peng Z H, Yin-Goen Q and Yang L 2008 *Nat. Biotechnol.* **26** 83
[10] Moskovits M 1978 *J. Chem. Phys.* **69** 4159
[11] Moskovits M 2005 *J. Raman Spectrosc.* **36** 485
[12] Park W H and Kim Z H 2010 *Nano Lett.* **10** 4040
[13] Ye G X, Michely T, Weidenhof V, Friedrich I and Wuttig M 1998 *Phys. Rev. Lett.* **81** 622
[14] Li L, Bao Z L, Ye X H, Shen J W, Yang B, Ye G X and Tao X M 2020 *Chin. Phys. Lett.* **37** 028102
[15] Shen J W, Ye X H, Bao Z L, Li L, Yang B, Tao X M and Ye G X 2020 *Chin. Phys. B* **29** 066801
[16] Xie J P, Yu W Y, Zhang S L, Chen M G and Ye G X 2007 *Phys. Lett. A* **371** 160
[17] Yu S J, Zhang Y J, Ye Q L, Cai P G, Tang X W and Ye G X 2003 *Phys. Rev. B* **68** 193403
[18] Lu C X, Cheng Y, Pan Q, Tao X M, Yang B and Ye G X 2016 *Sci. Rep.* **6** 19870
[19] Yang B, Ma R R, Li D M, Xia A G and Tao X M 2012 *Thin Solid Films* **520** 2321
[20] Zhang C H, Lv N, Zhang X F, Yang B and Ye G X 2011 *J. Phys.: Condens. Matter* **23** 435006
[21] Yang J L, Li R P, Han J H and Huang M J 2016 *Chin. Phys. B* **25** 083301
[22] Zeng Z, Liu Y Y and Wei J J 2016 *Trac-Trend Anal. Chem.* **75** 162
[23] Yang Z L, Chen S, Fang P P, Ren B, Girault H H and Tian Z Q 2013 *Phys. Chem. Chem. Phys.* **15** 5374
[24] Zhang X F, Zhang C H, Lv N, Xie J P and Ye G X 2010 *Chin. Phys. Lett.* **27** 096102
[25] Zhang P, Li Y, Wang D and Xia H 2016 *Part. Part. Syst. Charact.* **33** 924
[26] Zhao Y, Zhang Y J, Meng J H, Chen S, Panneerselvam R, Li C Y, Jamali S B, Li X, Yang Z L, Li J F and Tian Z Q 2016 *J. Raman Spectrosc.* **47** 662
[27] Solis D M, Taboada J M, Obelleiro F, Liz-Marzan L M and de Garcia A F J 2017 *ACS Photon.* **4** 329
[28] McMahon J M, Li S, Ausman L K and Schatz G C 2012 *J. Phys. Chem. C* **116** 1627
[29] Fang Y, Seong N H and D D D 2008 *Science* **321** 388
[30] Huang J, He Z, He X, Liu Y, Wang T, Chen G, Tang C, Jia R, Liu L, Zhang L, Wang J, Ai X, Sun S, Xu X and Du K 2017 *ACS Appl. Mater. & Interfaces* **9** 28902
[31] Qian L H and Chen M W 2007 *Appl. Phys. Lett.* **91** 083105